Journal of Nuclear Materials 417 (2011) 213–216
DOI: http://dx.doi.org/10.1016/j.jnucmat.2010.12.060

Microstructure and mechanical properties of ultrafine-grained Fe–14Cr and ODS Fe–14Cr model alloys

M.A. Auger [a,*], T. Leguey [a], A. Muñoz [a], M.A. Monge [a], V. de Castro [b], P. Fernández [c], G. Garcés [d], R. Pareja [a]

[a] Departamento de Física-IAAB, Universidad Carlos III de Madrid, 28911-Leganés, Spain
[b] Department of Materials, University of Oxford, OX1 3PH, United Kingdom
[c] National Fusion Laboratory-CIEMAT, Avda. Complutense 22, 28040 Madrid, Spain
[d] Departamento de Metalurgia Física, CENIM (CSIC), Avda. Gregorio del Amo 8, 28040 Madrid, Spain

Abstract: Reduced activation ferritic Fe–14 wt%Cr and Fe–14 wt%Cr–0.3 wt%Y_2O_3 alloys were produced by mechan-ical alloying and hot isostatic pressing followed by forging and heat treating. The alloy containing Y_2O_3 developed a submicron-grained structure with homogeneous dispersion of oxide nanoparticles that enhanced the tensile properties in comparison to the Y_2O_3 free alloy. Strengthening induced by the Y_2O_3 dispersion appears to be effective up to 873 K, at least. A uniform distribution of Cr-rich precipitates, stable upon a heat treatment at 1123 K for 2 h, was also found in both alloys.

1. Introduction

Fe–Cr binary alloys are nowadays the most promising base to fabricate reduced-activation ferritic/martensitic (RAFM) and ferritic (RAF) steels for structural applications in future fusion reactors as well as in generation IV fission reactors [1–3]. The reasons are their high resistance to swelling, helium embrittlement and irradiation creep, in combination with their mechanical prop-erties at elevated temperatures and corrosion resistance. However, conventional RAFM steels have limited the upper operating temperature to ~823 K because of their low thermal creep rupture strength above this temperature. A goal of fusion reactor designs is to enhance efficiency and safety by increasing the operating temperatures using fusion devices cooled by helium or liquid metals. This would require the development of RAFM/RAF steels with upper operating temperatures of ~923 K, at least. Oxide dispersion strengthening appears to have the capability to improve the elevated–temperature strength of high-chromium steels, thus increasing the operating temperatures up to ~950 K [4–7]. Consequently, the development of oxide dispersion strengthened (ODS) steels forces to investigate the effect of the fabrication and processing techniques on the mechanical behavior of ODS model alloys as well as to understand their strengthening mechanisms. The aims of the present work are: (1) to fabricate non-ODS and ODS Fe–14 wt% Cr alloys, via powder metallurgy methods, and (2) to investigate the effect of the processing parameters on their microstructure and mechanical behavior, in order to elucidate the oxide dispersion capacity for strengthening ferritic steels and extending their operating temperature window.

* Corresponding author. Tel.: +34 916249184; fax: +34 916248749.
E-mail addresses: mauger@fis.uc3m.es (M.A. Auger), leguey@fis.uc3m.es (T. Leguey), amunoz@fis.uc3m.es (A. Muñoz), mmonge@fis.uc3m.es (M.A. Monge), vanessa.decastro@materials.ox.ac.uk (V. de Castro), pilar.fernandez@ciemat.es (P. Fernández), ggarces@cenim.csic.es (G. Garcés), rpp@fis.uc3m.es (R. Pareja).

2. Experimental

Powder blends with target compositions: Fe–14%Cr and Fe–14%Cr–0.3%Y_2O_3 (wt%), hereafter designed respectively as reference Fe–14Cr and ODS Fe–14Cr, were mechanically alloyed at 300 rpm for 60 h inside a chromium steel vessel (11–12% Cr) under a He atmosphere in a highenergy planetary mill (Fritsch Pulverisette 6). Chromium steel balls (1–1.7% Cr, 10 mm diam.) with a ball-topowder mass ratio of 10:1 were used as grinding media. The alloyed powders were packed in 304 stainless steel cans (42 mm diam. × 57 mm height), degassed at 823 K for 24 h in vacuum and then the cans were vacuum sealed. The starting powders, as well as the blended and alloyed powders, were manipulated in each step of the procedure under Ar atmosphere inside a glove box. The canned powder was consolidated by hot isostatic pressing (HIP) for 2 h at 1373 K and a pressure of 200 MPa. The starting powders were spherical 99.7% pure Fe and 99.8% pure Cr powder, both with mean particle size <10 μm supplied by Alfa Aesar, and 99.5% pure monoclinic Y_2O_3 with particle sizes ⩽50 nm from Nanophase Technologies.

The cans containing the HIP consolidated alloys were forged into the form of ~12 mm × 12 mm × 170 mm bars. The forging temperature, which was 1323 K for reference Fe–14Cr, had to be increased to ~1373 K for ODS Fe–14Cr. After forging, the bars were heat treated at 1123 K for 2 h and air cooled. Finally, the remaining material coming from the can was removed. The chemical composition was

determined as follows: O and C contents in TC500 and CS600 elemental analyzers, manufactured by LECO Corporation; Y and Cr contents by X-ray fluorescence analysis. The microstructure was characterized by X-ray diffraction (XRD), laser diffraction, scanning and transmission electron microscopy (SEM and TEM), and energy dispersive spectroscopy (EDS). For microscopy characterization the following instruments were used: a Philips XL30 scanning electron microscope equipped with an EDAX (AMETEK, Inc., Materials Analysis Division) analyzer and TEM images were obtained with Philips CM20 and JEOL 3000F microscopes operated at 200 and 300 keV, respectively. Tensile tests in the temperature range 300–975 K at a constant crosshead rate of 0.1 mm/min were performed on flat tensile specimens with 20 mm gauge length × 3 mm width × 1 mm thickness cut parallel to the bar axis. Above room temperature, the tests were performed with the specimens under a flow of pure Ar. In addition, Vickers microhardness was measured using an applied load of 300 g for 20 s.

3. Results and discussion

3.1. Chemical composition and density

Table 1 shows the chemical composition of the starting elemental powders and the HIP consolidated alloys after forging and heat treating. The compositional analyses indicated a significant Fe enrichment in the alloys, attributable to the observed Cr sticking on the grinding media surface. Under the present processing conditions, no significant intake of O and C appears to occur. The high oxygen content in the Fe and Cr starting powders is responsible of the oxygen content measured in the consolidated alloys. This may induce a detrimental effect on the mechanical properties.

The average particle size of the alloyed powders before canning, determined from SEM and laser diffraction analyses, is given in Table 2. This value was found to be 18% smaller in the ODS alloy than in the reference Fe–14Cr alloy.

The measured densities for the forged and heat treated materials are shown in Table 2. The density for the ODS Fe–14Cr alloy results in a higher value than the one for the reference Fe–14Cr alloy. This result can be related to the finer grain size developed in the ODS alloy.

3.2. Microstructure

3.2.1. Fe–14Cr

TEM observations of the Fe–14Cr alloy after forging and heat treating at 1123 K revealed a duplex microstructure formed by large ferrite grains with sizes in the range 3–7 μm, and regions containing submicron ferrite grains with an average size of ~380 nm, as Fig. 1a shows. A dispersion of Cr-rich precipitates with sizes ranging between 50 and 400 nm were found distributed inside the large ferrite grains and aligned along the grain boundaries, besides small voids which would very likely contain entrapped gas, as Fig. 1b reveals. EDS and electron diffraction analyses suggested that the nature of these Cr-rich precipitates may differ in structure and composition. In addition to Cr and Fe, these particles contained C, N, O and other impurities. A detailed study of the microstructure of these alloys and nature of the precipitates are reported in [8].

Table 1
Chemical composition of the starting elemental powders and HIP consolidated alloys, measured after forging and heat treating at 1123 K (Fe mass balance).

	O (wt%)	C (wt%)	Y (wt%)	Cr (wt%)
Fe powder	0.28	0.02	–	–
Cr powder	0.67	0.006	–	99.81
Fe–14Cr	0.36 ± 0.01	0.07 ± 0.01	–	13.1 ± 0.1
ODS Fe–14Cr	0.54 ± 0.11	0.05 ± 0.01	0.20 ± 0.01	13.4 ± 0.1

Table 2
Average particle size of the milled powders and characteristic parameters for the HIP consolidated alloys after forging and heat treating.

Alloy	Powder particle size (μm)	Density (g/cm^3)	Average crystallite size (nm)	Accumulated strain	Microhardness (GPa)
Fe–14Cr	44.69	7.654	22	3.1	2.71 ± 0.04
ODS Fe–14Cr	36.68	7.711	16	4.5	4.17 ± 0.05

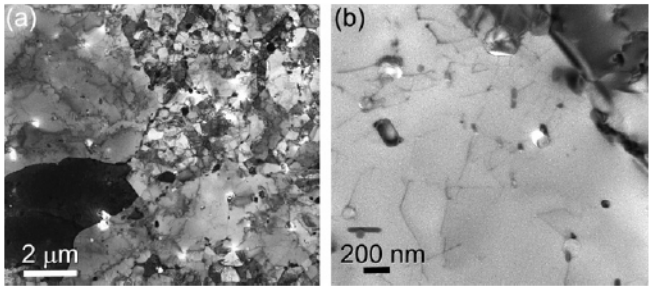

Fig. 1. TEM images of the reference Fe–14Cr alloy forged and heat treated at 1123 K. (a) Duplex microstructure. (b) Dispersion of Cr-rich precipitates and voids.

3.2.2. ODS Fe–14Cr

Fig. 2a shows the microstructure of the ODS Fe–14Cr alloy after forging and heat treating. It exhibited a homogeneous submicron structure of ferritic grains, apparently unrecovered, with an estimated average size of ~360 nm. Alike the reference Fe–14Cr, a fine uniform distribution of Cr-rich precipitates is found in the ferritic matrix. The TEM/EDS analyses did not show traces of Y in these particles. Also, the TEM analyses revealed the presence of a dispersion of Y–O rich nanoparticles, as shown in Fig. 2b. Voids were also observed in ODS Fe–14Cr, frequently associated to the nanoparticles [8].

3.3. XRD measurements

XRD patterns from both alloys showed a single ferrite phase. The lattice parameter determined for the ODS Fe–14Cr in forged-heat treated condition was 0.7% larger than the one corresponding to the reference Fe–14Cr. These calculations were made by a least squares fitting of the XRD data using the WINPLOTR software [9]. The average crystallite size and accumulated strain were estimated from the analyses of the width and shape of the diffraction peaks, by applying the De Keijser formula [10] included in WINPLOTR

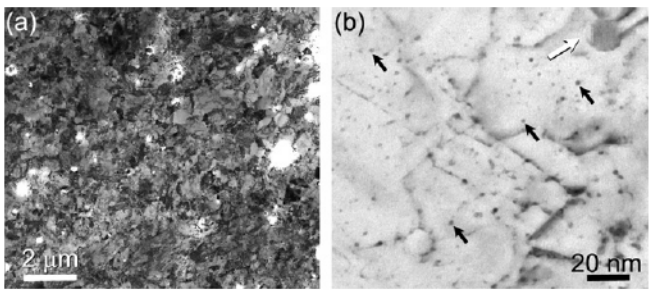

Fig. 2. TEM images of the ODS Fe–14Cr alloy forged and heat treated at 1123 K. (a) Submicron-grained structure. (b) Dispersion of Y–O rich nanoparticles (black arrows). Void attached to a nanoparticle is marked by a white arrow.

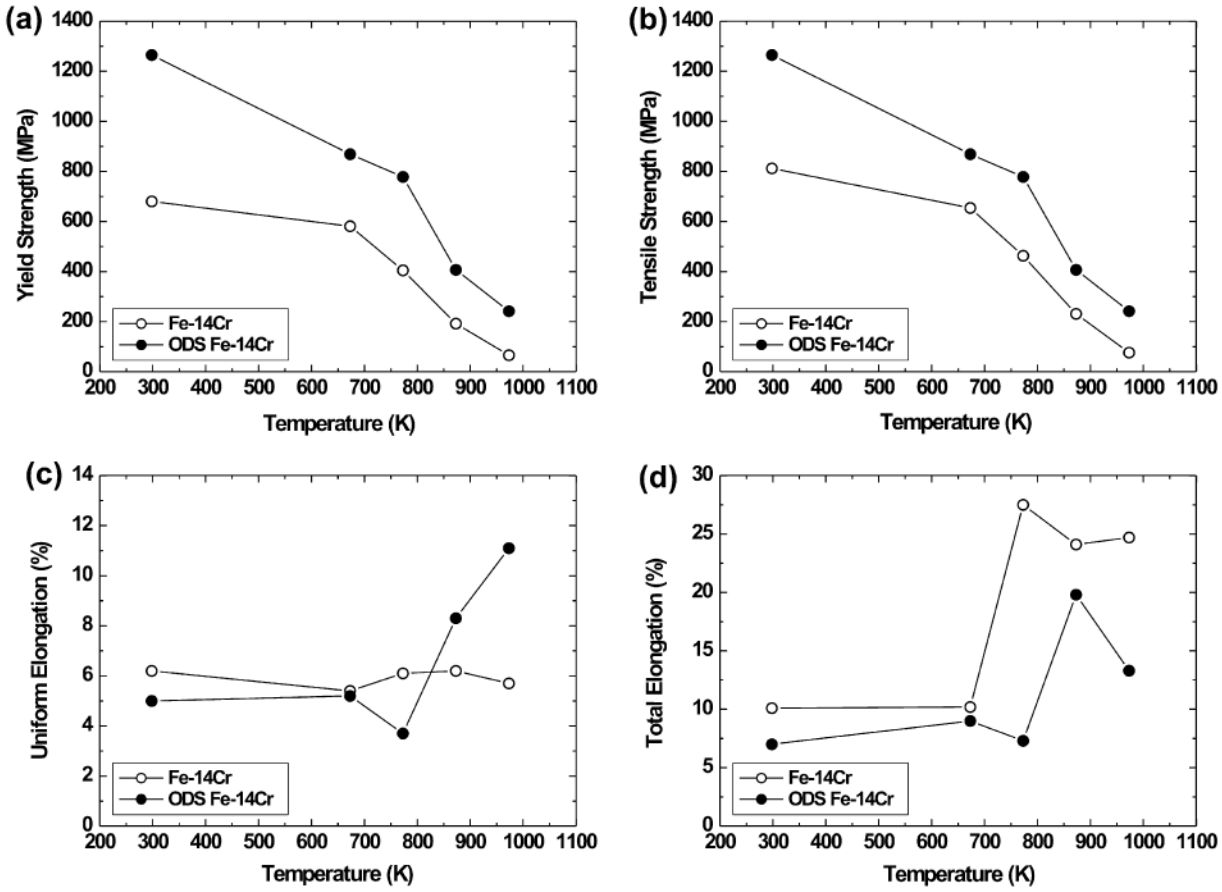

Fig. 3. Tensile properties for the HIP consolidated alloys in the forged-heat treated condition.

software [9] processing. Table 2 shows these values for both alloys in the forged-heat treated condition. The XRD results in conjunction with the TEM observation indicated that the fine Y–O rich nanoparticle dispersion had the capability of promoting and retaining grain refinement upon forging and subsequent heat treatment at 1123 K. Also, the Cr-rich particles should have a role in constraining recovery and grain growth as the results for refer-ence Fe–14Cr suggested.

3.4. Mechanical properties

The tensile properties for the alloys in the forged-heat treated condition are summarized in Figs. 3 and 4. The tensile properties for the ODS Fe–14Cr alloy in the range 300973 K were remarkably enhanced in relation to those for the reference Fe–14Cr alloy. The enhancement factor of the yield strength in the ODS alloy compared to the one in the non-ODS alloy was of ~1.7 at room temperature but 2.6 at 973 K. The fact that this enhancement is higher with increasing temperature is a very interesting result. It demonstrates the real capability of the nanoparticle dispersion in combination with the submicron-grained structure, for strengthening a ferritic matrix up to 873 K, at least. Moreover, Fig. 4 discloses a very interesting characteristic of the ODS Fe–14Cr in relation to the non-ODS counterpart alloy. The hardening ratio, defined as ten-sile strength/yield strength, appears to increase steeply in the ODS Fe–14Cr at temperatures above 773 K, while it does not exhibit a defined trend in the reference Fe–14Cr. Another relevant characteristic of the ODS Fe–14Cr compared to the non-ODS counterpart alloy is the shift in the onset of the sharp drop of flow stress, from ~673 K to ~773 K, coinciding with a sharp increase of the uniform

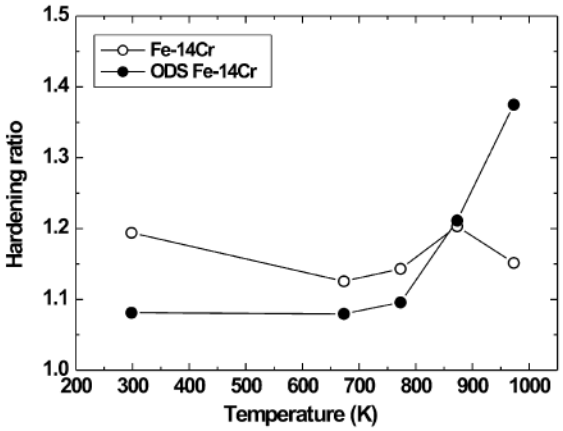

Fig. 4. Hardening ratio as a function of temperature for the HIP consolidated alloys in the forged-heat treated condition.

elongation and hardening ratio, which are not observed in the non-ODS alloy.

The microhardness results shown in Table 2 also reflect the capability of the nanoparticle dispersion to strength and stabilize the grain structure of ferritic Fe–14Cr alloys. The fact that the ODS alloy required a higher temperature to be forged compared to that for the non-ODS alloy, as well as the considerable effect of forging on the microstructure and microhardness, demonstrate that the grain growth during the HIP treatment and subsequent

thermomechanical treatments is mainly controlled by the presence of the Y–O rich nanoparticles in the alloyed powder.

4. Conclusions

The addition of Y_2O_3 to the Fe–14Cr blend appears to promote particle size refinement of the mechanically alloyed powder and favors its densification. The fabrication and processing route herein applied produced an ODS ferritic Fe–14Cr alloy with a submicron-grained structure and a dispersion of Y–O rich nanoparticles and Cr-rich precipitates.

The Y–O rich dispersion is responsible for the enhancement of the tensile properties, grain refinement and stability of the induced structure. This submicron-grained structure was stable upon heat treatment at 1123 K. The ODS ferritic Fe–14Cr alloy fabricated and processed under the present conditions appears to exhibit superior tensile properties than ODS Fe–17Cr alloys processed by extrusion followed by rolling and annealing [5] and the ODS (12–14)Cr2WTi ferritic steels fabricated and processed by a similar route [11].

Acknowledgements

This investigation was supported by the Spanish Ministry of Science and Innovation (project No ENE 2008-06403-C06-04 and Juan de la Cierva program), the Comunidad de Madrid through the program ESTRUMAT-CM (grant S0505/MAT/0077), and the European Commission through the European Fusion Development Agreement (contract No. 09-240), the IP3 FP6 ESTEEM project (contract No. 026019) and the Fusion Energy Materials Science (FEMaS) FP7 coordination action. All the fundings are gratefully acknowledged.

References

[1] R.L Klueh, D.R Harries, High-Chromium Ferritic and Martensitic Steels for Nuclear Applications, ASTM, West Conshohocken, PA, 2001.
[2] L.K. Mansur, A.F. Rowcliffe, R.K. Nanstad, S.J. Zinkle, W.R. Corwin, R.E. Stoller, J. Nucl. Mater. 329–333 (2004) 166–172.
[3] N. Baluc, R. Schäublin, P. Spätig, M. Victoria, Nucl. Fusion 44 (2004) 56–61.
[4] S. Ukai, M. Fujiwara, J. Nucl. Mater. 307–311 (2002) 749–757.
[5] I.S. Kim, T. Okuda, C.Y. Kang, J.H. Sung, P.J. Maziasz, R.L. Klueh, K. Miyahara, Met. Mater. 6 (2000) 513–518.
[6] R. Lindau et al., Fusion Eng. Des. 75–79 (2005) 989–996.
[7] R.L. Klueh, J.P. Shingledecker, R.W. Swindeman, D.T. Hoelzer, J. Nucl. Mater. 341 (2005) 103–114.
[8] V. de Castro, T. Leguey, M.A. Auger, S. Lozano-Perez, M.L. Jenkins, J. Nucl. Mater. 417 (2011) 217–220.
[9] T. Roisnel, J. Rodriguez-Carvajal, Mater. Sci. Forum 378–381 (2001) 118–123.
[10] T.H. De Keijser, J.I. Langford, E.J. Mittemeijer, A.B.P. Vogels, J. Appl. Crystallogr. 15 (1982) 308–314.
[11] Z. Oksiuta, N. Baluc, Nucl. Fusion 49 (2009) 055003. 9pp..